Intense Laser Alignment As a Route to Control of Surface Reactions

Deepika Shreenivas,[†] Anthony Lee,[†] Nadine Walter,[‡] David Sampayo,[§] Steve Bennett,[†] and Tamar Seideman*

Department of Chemistry, Northwestern University, 2145 Sheridan Road, Evanston, Illinois 60208-3113

Received: December 20, 2009; Revised Manuscript Received: March 1, 2010

We explore the possibility of controlling the orientation of adsorbates, and their adsorption site, through alignment of a beam of gas-phase molecules prior to the surface reaction. To that end, we carry out classical trajectory simulations using ab initio data for the specific example of the I_2/Si(100) adsorption reaction. I_2 is found to adsorb with the molecular axis roughly parallel to the surface plane independently of the initial alignment. The orientation of the molecule in the surface plane and the adsorption site are controllable through alignment of the gas-phase projectiles. Our results are explained in terms of the surface properties and the reaction dynamics, and the extent to which and way in which they may be generalized is discussed.

I. Introduction

The development of means of producing aligned molecular layers on solid substrates may reward a variety of areas of science and technology. These include molecular electronics, controlled crystallography, structural determination of biological molecules, understanding of organic interfaces, and the development of advanced materials with preferred electric, magnetic, optical, or mechanical properties. The reaction of aligned gas-phase molecules with a substrate as a route to that end is of interest also from a chemical perspective, and its realization has been a major goal of early stereodynamical studies.[1] The early alignment techniques of stereodynamics were found inadequate to achieve this goal due to either or both insufficiently sharp alignment or the presence of a strong field. The advance of postpulse nonadiabatic alignment by means of a short (or a rapidly truncated), moderately intense laser pulse during the past decade[2−9] suggests an opportunity to return to the surface application in a new context.

In remotely related research, the drive toward further device miniaturization has been fruitful in motivating the study of a variety of new and fascinating phenomena introduced when material systems are brought down to the nanoscale as well as the development of methods of combining molecules with solids to make nanoscale electronic, photonic, and electromechanical devices. Currently available techniques toward device miniaturization are conventionally divided into two categories, bottom-up techniques, wherein individual molecules are assembled into functional devices, and top-down techniques, wherein ever smaller features are etched or deposited onto suitable substrates.

Within the second category, ref 10 proposed the possibility of using intense-laser molecular optics as a route to nanoscale deposition onto, and etching of, substrates. An approach for laboratory demonstration of this scheme is detailed in ref 11. Strong-field molecular optics employs the natural intensity gradient of laser beams to manipulate the center-of-mass motion of molecules in physical space. In the long-wavelength limit (that is, at laser frequencies well below electronic transition frequencies), a molecular beam traversing the intense laser beam is deflected toward the high-intensity region due to the spatially inhomogenous interaction of the field with the molecular polarizability tensor. By proper choice of the relative location of the laser and molecular beams, the molecular trajectories can be thus brought to a focus in a predetermined spot in space; the laser serves as a lens for the molecular motion.

The possibility of placing a surface at the focus so as to deposit nanoscale features is inviting as the ratio of the laser focus to the molecular focus (the lateral extend of the focused molecular beam) translates into the factor of reduction of the deposited features with respect to the diffraction limit. In the case of molecules that react with the substrate, one might envision using a second laser pulse to remove the reacted nanofeatures, thus providing a route to nanoscale etching. The method offers potentially several attractive features. (i) Molecular optics is very general; since all atoms and molecules are polarizable, it is possible to manipulate any species that could be entrained in a molecular beam. (ii) As an approach toward nanopatterning, the method offers a significant reduction of the feature size beyond the diffraction limit. (iii) Complex patterns can be produced while maintaining the write rate of optical methods. (iv) The approach offers, in principle, the possibility of depositing aligned nanostructures with anticipated interesting electric and optical properties. The last feature is considered the most attractive potential advantage of the molecular optics approach, which distinguishes it from other methods, whose success has already been demonstrated experimentally. It is also the most interesting feature as it introduces several new questions for formal and numerical research.

A number of these questions have been discussed in the recent literature. One question regards the possibility of retaining the laser-induced alignment after the molecules have exited the laser beam and have reached the focus, where the surface is placed. It has been demonstrated, formally, numerically, and experimentally, that laser alignment survives after turn-off of the field−matter interaction provided that the turn-off of the interaction is nonadiabatic (fast as compared to rotational periods). In this case, a broad rotational wavepacket is produced that aligns at a controllable delay with respect to the peak of the interaction and, after dephasing, is periodically reconstructed.

* To whom correspondence should be addressed. E-mail: t-seideman@northwestern.edu.

[†] A NRC undergraduate summer student.

[‡] A MRSEC undergraduate summer student.

[§] A SROP undergraduate summer student.

10.1021/jp9120113
Published on Web 04/22/2010

Thus, transient alignment is available periodically in time under field-free conditions. In order, however, to focus molecular beams, a long (with respect to rotational periods) interaction time is essential. Thus, to combine focusing with field-free alignment, one requires a pulse that adiabatically turns on and suddenly turns off. The coupled rotational−translational molecular dynamics that is induced by such interaction is studied within a hybrid quantum classical approach in ref 12, where the quality of the associated alignment and focusing is assessed. An experimental demonstration of the production and application of slowly turning on, suddenly turning-off pulses is described in ref 13. Use of the transient alignment that is available at the rotational revivals for nanolithography is likely to be complicated, if possible, since the velocity of molecular beams has a finite distribution. We note, however, that the average alignment after nonadiabatic turn-off of the interaction does not vanish. It is readily shown analytically[14] that the long time average of the expectation value of $\cos^2\theta$ in the wavepacket (θ being the polar angle between the molecular and field polarization axes), the most commonly used parameter to characterize alignment, is not 1/3 as in the isotropic limit but rather 1/2. That residual alignment is sufficient for our present purpose. Other questions associated with the application of intense-field molecular optics to nanoprocessing are addressed in ref 11, where an experimental realization of the method is described in detail.

A problem of significant chemical interest is the effect of the surface reaction on the alignment and the focusing of the gas-phase molecular beam. A closely related question, the topic of a substantial body of research in the context of stereodynamics,[1,15] is the effect of the alignment and the focusing on the outcome of the surface reaction. The objective of the present work is to address these issues by means of numerical simulations of a simple surface reaction that is numerically and experimentally accessible. Specifically, we consider the collision of I_2 molecules with a Si(100) surface within the classical trajectory approximation. The reason for our choice of system is three-fold. I_2 has a relatively high polarizability, and its focusing dynamics have been studied both numerically[10,16] and experimentally.[17] The (001) crystal face of silicon is the starting point for almost all integrated circuits used for microprocessors and memory chips; hence, understanding and learning to control the chemistry of this surface is relevant. Furthermore, I_2 reacts readily with the dangling bonds of the Si(100) surface, forming stable Si−I bonds. On the other hand, the Si−I bonds formed upon collision can be cleaved by a second laser pulse. This introduces the possibility of employing molecular optics for selective nanoscale etching. We remark, however, that the I_2/Si(100) system serves here as a simple model to explore an idea that, we hope, has more general validity. Our goal is thus narrowly defined, and hence, we focus entirely on the mutual effects of the gas-phase alignment and the surface reaction and do not explore other aspects of the I_2/Si(100) dynamics in any detail.

It is worth noting that the I_2/Si(100) system does not make an ideal model for control over the orientation of the deposited features via alignment of the gas-phase molecular beam. This follows from the highly corrugated nature of the Si(100) surface that tends to dictate the configuration of adsorbates. A smoother surface, such as a metal, is expected to serve better to that end. Thus, it is clear that an I_2 molecule would not adsorb perpendicular to the Si(100) surface, irrespective of its initial alignment. Nonetheless, we find that the orientation of the molecular axis in the surface plane is controllable through alignment of the gas-phase incident beam. Our results suggest also that alignment of the gas-phase species can serve to eliminate or reduce the scatter of adsorbates among several reaction sites that is found with randomly oriented species.

Although our interest is not in the specifics of the I_2/Si(100) collision, it is appropriate to briefly review here some of the experimental and numerical work on this and analogous silicon surface halogenation reactions. Fluorination of the Si(100) surface has been the most thoroughly investigated of the silicon surface halogenation reactions, driven largely by its relevance to the fabrication of microelectronic devices through plasma etching. In particular, the reaction of F_2 molecules with a Si(100)-2 × 1 surface was studied in considerable detail, both experimentally[18−20] and through molecular dynamics simulations.[21−28] These studies generated considerable insight into the F_2/Si collision dynamics while developing a useful approach to the generation of a gas−surface potential energy surface based on isolated-molecule-like quantum chemistry calculations. The reaction of Cl_2 with silicon surfaces was addressed experimentally in refs 29−31 and numerically in refs 32−34, whereas the bromination process was studied in ref 35.

Experimental studies of the I_2/Si(100)-2 × 1[36−38] collision system have illustrated that I_2 dissociates and chemisorbs to Si dimer dangling bonds at room temperature, noting the role played by steric hindrance in determining the resulting structure. The I_2/Si(111)-7 × 7 reaction was likewise experimentally shown to result in dissociative adsorption, in this case forming a mixture of moieties of which SiI dominates. Although the I_2/Si collision has been studied much less extensively than the F_2 analogue, several experiments suggest the potential interest in this reaction from the fundamental material science perspective. Reference 39 illustrates the application of I-terminated surfaces as as alternative to the conventional use of H-terminated analogues for photochemical patterning and modification. In this study, the attachment of I atoms to the Si surface is done in a benzene solution, but the proposed applications are independent of the preparation details. An earlier investigation of Si passivation by I atoms was presented in ref 40. A related study[41] illustrates unusual adsorbate ordering effects in coadsorption of I and H atoms on the Si(100) surface. More recent investigations of surface patterning of I−Si(100) found an interesting I-destabilization and roughning of the surface.[37] A general review of spontaneous halogen etching of Si(100) and Si(111) surfaces is given in ref 42. Finally, we note an only remotely related, but very interesting, series of studies on the localized nature of surface reactions on silicon surfaces, where halogenation products are found to pattern the surface following the orientation of the initially adsorbed molecular state.[43,44]

In the next section, we outline our method of constructing a potential energy surface for the I_2/Si(100) system and studying the reaction dynamics subject to that potential. Section III presents and discusses the numerical results, and the final section summarizes our conclusions.

II. Numerical Method

The reaction of the focused and aligned molecular beam with the Si(100) surface is studied with standard and well-documented[45] methods of reaction dynamics that are only briefly outlined in this section. At the outset, we make three approximations. We assume Born−Oppenheimer separability of the electronic and nuclear modes, we use an approximate, closed-form expression for fitting an ab inito potential energy surface for the nuclear modes, and we study the dynamics subject to this potential within classical mechanics.

Our method of constructing a potential energy surface is similar to that employed in extensive studies of the reaction of

F_2 with Si(100).[21−28] Ab initio data at the CASPT2:CASSCF IMOMO level (complete active space second-order perturbation theory:compete active space space-self-consistent field-integrated molecular orbital and molecular orbital)[46] is fitted to the functional form developed by Stillinger and Weber[21] for describing the F_2/Si(100) potential energy surface. This two- and three-body potential was found successful in several molecular dynamics simulations, a number of which reported direct comparison with experiment, and serves well our present purpose. We remark, however, that (in the lowest-energy configuration) it does not exhibit buckling of the Si(100) dimers. A minor modification of the Stillinger−Weber form was introduced in refs 22 and 23 and is used also in the present study. In addition, the terms denoted h_{SiXX} and h_{XSiX} (X being a halogen), which involve one silicon and two halogen atoms, were omitted as we found that for the I_2/Si(100), the fit quality deteriorates by their inclusion. We expect that this result is due to the substantially larger size of the I_2 ($r_{eq,I_2} = 2.666$ Å) as compared to the size of the F_2 ($r_{eq,F_2} = 1.4$ Å) molecule.

Our potential energy surface is thus

$$V = \sum v_{Si-Si} + \sum v_{I-I} + \sum v_{Si-I} + \sum v_{Si-Si-Si} + \sum v_{Si-Si-I} \quad (1)$$

where

$$v_{Si-Si} = \begin{cases} A_{Si-Si}(B_{Si-Si}r^{-4} - 1)e^{(r - a_1)^{-1}} & \text{for } 0 < r < a_1 \\ 0 & \text{for } r > a_1 \end{cases} \quad (2)$$

$$v_{I-I} = D_e[(e^{-\alpha(r-r_{eq})}) - 1]^2 - D_e \quad (3)$$

$$v_{Si-I} = \begin{cases} A_{Si-I}(B_{Si-I}r^{-3} - r^{-2})e^{\gamma_{Si-I}(r - a_2)^{-1}} & \text{for } 0 < r < a_2 \\ 0 & \text{for } r > a_2 \end{cases} \quad (4)$$

$$v_{ABC} = h_{ABC}(r_{AB}, r_{BC}, \theta_B) + h_{BCA}(r_{BC}, r_{CA}, \theta_C) + h_{CAB}(r_{CA}, r_{AB}, \theta_A) \qquad A, B, C = Si, I \quad (5)$$

$$h_{Si-Si-Si} = \begin{cases} A_{Si-Si-Si}\left(\cos\theta + \frac{1}{3}\right)^2 e^{\gamma_{Si-Si-Si}[(r - a_1)^{-1} + (s - a_1)^{-1}]} & \text{for } 0 < r < a_1 \\ 0 & \text{for } r > a_1 \end{cases} \quad (6)$$

$$h_{Si-Si-I} = \begin{cases} A_{Si-Si-I}\left[\left(\cos\theta + \frac{1}{3}\right)^2 - c_{Si-Si-I}\right] \times e^{\gamma_{Si-Si-I}[(r - a_2)^{-1} + (s - a_2)^{-1}]} & \text{for } 0 < r < a_2 \\ 0 & \text{for } r > a_2 \end{cases} \quad (7)$$

$$h_{Si-I-Si} = \begin{cases} A_{Si-I-Si}e^{\gamma_{Si-I-Si}[(r - a_2)^{-1} + (s - a_2)^{-1}]} & \text{for } 0 < r < a_2 \\ 0 & \text{for } r > a_2 \end{cases} \quad (8)$$

with all parameters collected in Table 1. The top eight parameters of Table 1 were fixed to their literature value, and the bottom nine were extracted through a fit to the ab initio data of ref 46.

TABLE 1

Parameters from Literature	
A_{Si-Si}	352.478 kcal/mol
B_{Si-Si}	11.603 Å^4
a_1	3.771 Å
D_e	35.835 kcal/mol
α	1.866 Å^{-1}
r_{eq}	2.666 Å
$A_{Si-Si-Si}$	1050.00 kcal/mol
$\gamma_{Si-Si-Si}$	2.514 Å
Parameters from Fit to Ab Initio Calculation[46]	
$A_{Si-Si-I}$	358.361 kcal/mol
$C_{Si-Si-I}$	0.272
$\gamma_{Si-Si-I}$	2.289 Å
$A_{Si-Si-I}$	8970.640 kcal/mol
$\gamma_{Si-Si-I}$	5.427 Å
A_{Si-I}	20977.229 kcal/mol Å^2
B_{Si-I}	1.885 kcal/mol Å
γ_{Si-I}	7.205 Å
a^2	4.714 Å

Proceeding to develop a model for the silicon surface, we first construct a 12-layer slab consisting of 429 atoms and optimize its structure through energy minimization, starting with the Stillinger−Weber structure. In this procedure, the bottom layer is held fixed at the equilibrium bulk configuration, so as to mimic the bulk solid. The optimized structure is employed in constructing a I_2−Si(100) model to be used in the dynamical simulations. The surface reaction on the Si(100) surface is a localized event since the surface is rather corrugated. Hence, a much smaller slab is required to capture the dynamics than that needed to optimize the structure. Here, we use a 5-layer slab consisting of 60 atoms per layer. The atoms of the top four layers are permitted to move freely, whereas those constituting the bottom layer are held fixed at the optimized equilibrium configuration. Periodic boundary conditions are used in the lateral dimensions to mimic the infinite surface. The slab is replicated 8 times so as to surround the primary 300 atom zone by 8 images in the lateral directions. The Si atoms in the secondary zones are permitted to interact with those of the primary zone but not with the incident I_2 molecule. The slab dimensions are determined in a series of preliminary calculations, where we vary the number of layers and the number of atoms per layer to achieve convergence.

The reaction dynamics is followed by solving Hamilton's equations for the 1452-mode system using Adam's predictor−corrector algorithm.[45] This approach has the merit of speed, and its accuracy, while not matching that of other algorithms, is adequate for our present purpose.

III. Results and Discussion

Figure 1 shows the top layer of our (primary zone) silicon slab and defines our choice of coordinate system. We follow the standard convention of choosing the *z*-axis parallel to the surface normal and define the *y*-axis by a vector parallel to the Si_2 dimer axes. The distances marked by capital letters in Figure 1 are provided in the figure caption for reference below. We introduce two sets of angles with respect to the Cartesian system of Figure 1. The orientation of the I_2 axis is defined by the polar and azimuthal angles (Θ, Φ), whereas the direction of the center-of-mass velocity vector is defined by the polar and azimuthal angles (Θ_{cm}, Φ_{cm}). The polar angle is the angle between each

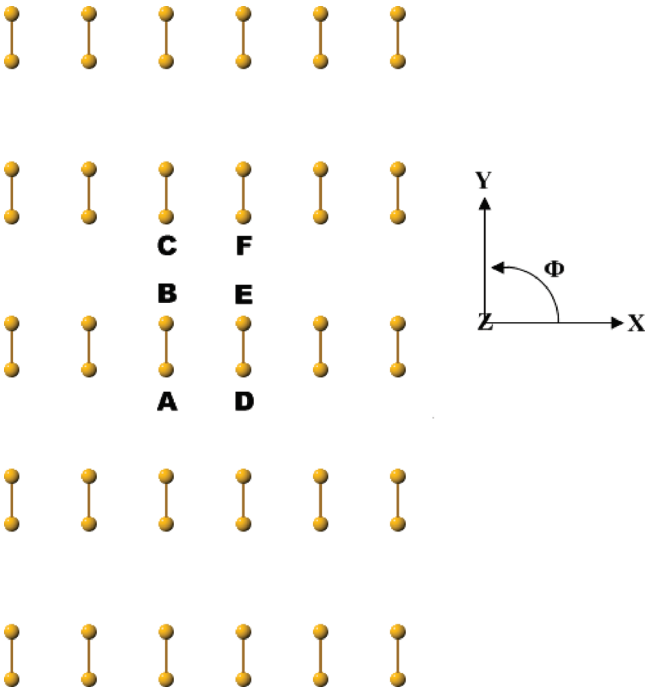

Figure 1. The top layer of the primary zone silicon slab used in the structural and dynamical calculations. The z-axis is defined by the surface normal, and the y-axis is defined by the Si_2 dimer axes, with the origin of coordinates taken to be the midpoint of the centers of two dimers. The distances marked by capital letters are R(A−B) = 2.405 Å, R(A−D) = 3.837 Å, R(A−E) = 4.528 Å, R(B−C) = 5.269 Å, and R(B−F) = 6.518 Å.

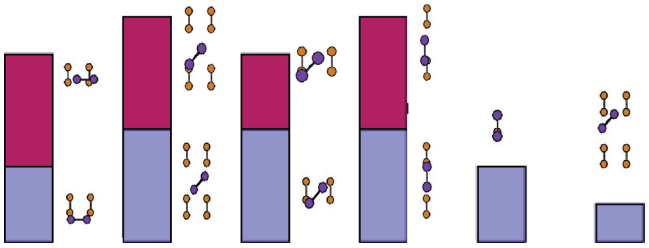

Figure 2. Schematic illustration of the adsorption configurations found to result from the I_2/Si collision. The icons are provided to assist in the interpretation of Figures 3−8, whereas the bars serve as a glossary for Figure 9.

vector and the surface normal, and the azimuthal one is the angle between the projection of the vector onto the xy-plane and the x-axis. The origin of the coordinate systems is taken to be the center of the midpoint of two silicon dimers (the center of the rectangle marked A−B−E−D in Figure 1).

Before proceeding to discuss the results of our molecular dynamics simulations, it is helpful to briefly consider the form of the potential energy surface, which participates in determining these dynamics. To assist the discussion, we provide in Figure 2 schematic illustrations of the adsorption configurations that we found in trajectory calculations to result from I_2 collision with the surface. The icons of Figure 2 serve as a glossary for description of the structural and dynamical results below. The associated bars connect this discussion with the statistical results of Figure 9. Since the molecule is roughly parallel to the surface upon adsorption (vide infra), we focus on configurations where $\Theta = \pi/2$ and examine the role played by the remaining parameters. Figure 3 shows the I_2/Si(100) interaction potential of eq 1 as a function of the x- and y-center-of-mass coordinates of the molecule, (X_{cm}, Y_{cm}), at a fixed height, $Z_{cm} = 2.5$ Å, above the surface. The molecule is oriented parallel to the surface,

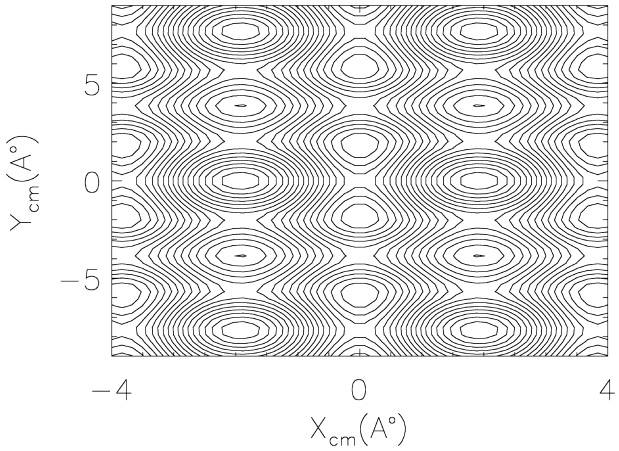

Figure 3. The I_2/Si(100) interaction potential of eq 1 as a function of the x- and y-center-of-mass coordinates of the molecule, (X_{cm}, Y_{cm}), at a fixed height, $Z_{cm} = 2.5$ Å, above the surface. The molecule is oriented parallel to the surface, along the Si_2 dimer axes.

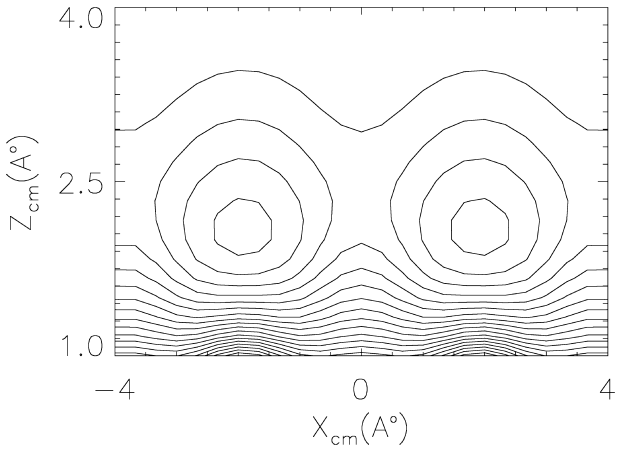

Figure 4. The dependence of the potential energy surface on the I_2 x- and z-center-of-mass coordinates. The molecule is oriented at ($\Theta = \pi/2$, $\Phi = \pi/2$) as in Figure 3, and its center of mass is fixed at $Y_{cm} = 2.1$ Å.

along the Si_2 dimer axes, $\Phi_{cm} = \pi/2$. The minima of Figure 3 correspond to the location of closest approach of the I atoms to the underlying Si atoms as at this distance above the surface, attractive forces dominate. Figure 4 complements Figure 3 with a view of the dependence of the potential energy surface on the I_2 x- and z-center-of-mass coordinates. The molecule is oriented at ($\Theta = \pi/2$, $\Phi = \pi/2$) as in Figure 3, and its center of mass is fixed at $Y_{cm} = 1.2$ Å, corresponding to motion of the molecule above a silicon atom row (see Figure 1). The periodic potential wells along the x-axis at $Z_{cm} = 2.1$ Å and the strong repulsion at $Z_{cm} \lesssim 1.6$ Å correspond to location of the molecule above a Si atom. For $Z_{cm} > 3.5$ Å, the potential is essentially independent of height above the surface.

Most relevant for our present study is the form of the potential energy surface as a function of the molecular orientation in the xy-plane. This view is presented in Figure 5, where the center-of-mass location in the xz-plane is fixed at $Z_{cm} = 3.5$ Å, $X_{cm} = 1.9184$ Å = (1/2)R(A−D) in Figure 1, corresponding to motion of the center of mass above the silicon dimers across three dimer rows. The global minima along the Y_{cm} axis are found where the I_2 center of mass is above the center of a Si_2 dimer as this configuration optimizes the attractive interaction of both I atoms with the Si atoms. Local minima in Y_{cm} are found where the I_2 center of mass is located between two dimer rows, permitting interaction with both dimers. The increased stability of the

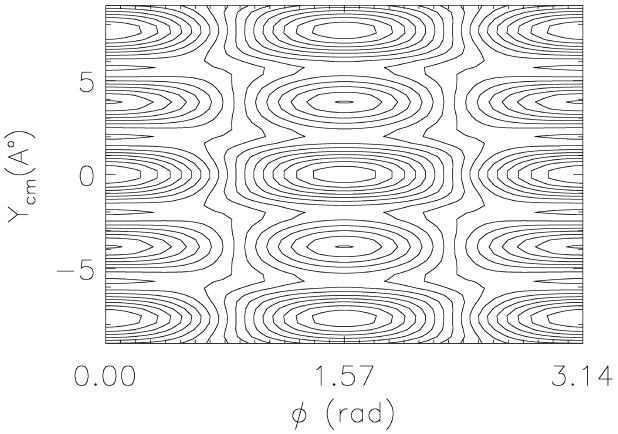

Figure 5. The dependence of the potential energy surface on the I_2 *y*-center-of-mass coordinate and the azimuthal angle of orientation of the molecule, Φ. The center-of-mass location in the *xz*-plane is fixed at $Z_{cm} = 3.5$ Å, $X_{cm} = 1.9184$ Å $= (1/2)R$(A−B) (Figure 1), and $\Theta = \pi/2$.

former configuration is due to the better size match of the I_2 bond length ($r_{eq} = 2.666$ Å) with the Si_2 dimer length (2.41 Å on our potential energy surface) than that with the inter-row distance (5.27 Å). For the same reason, minima along the Φ coordinate are found at $\Phi = \pi/2, 3\pi/2$, corresponding to parallel orientation of the I_2 axis with respect to the dimer axis. Clearly, this picture is reversed when the center of mass is located between dimers, $X_{cm} = 0$, where global minima in the Φ direction are found at $\Phi = 0, \pi$. The energy gap between the maxima and minima of Figure 5 is 1.3 eV with the molecular center of mass above the midpoint of a dimer (configuration V in Figure 2) and 1.2 eV with the molecular center of mass above the midpoint between two dimers (configuration IV in Figure 2). One-dimensional views of the potential energy surface versus Φ are provided in the Supporting Information section.

The gross features of the surface reaction subject to the potential energy surface of Figures 3−5 can be readily predicted based on energetic considerations. The Si−I bond energy is roughly 3 eV (see Figure 6 for quantification of this statement), whereas the I−I bond energy is roughly 1.6 eV. Thus, dissociative adsorption is expected to be exothermic. We note, however, that the gas-phase I_2 potential energy curve remains bound up to ∼9.6 Å, supporting over 110 vibrational levels.[47] Thus, molecular adsorption forming two Si−I bonds without breakage of the I−I bond is energetically preferred and numerically found at zero surface temperature, although at finite surface temperatures, it is not expected. For the purpose of the present work, it matters little if the molecule dissociates or remains intact upon adsorption. The pattering of the surface follows the initial orientation in both cases and is determined by the gas-phase alignment in the same way; see also ref 43. Figures 6 and 7 classify the adsorption configurations found in our dynamical simulations into five categories (schematic ball and stick models of these configurations are provided in Figure 2). In each of the figures, panel (I) corresponds to I_2 attachment parallel to the dimer rows (left icon in Figure 2), panel (II) corresponds to diagonal attachment, with the I_2 bridging two dimer rows (second to left icon in Figure 2), panel (III) corresponds to diagonal attachment along a single dimer row (third icon in Figure 2), panel (IV) depicts adsorption perpendicular to the rows, bridging two rows (fourth icon in Figure 2), and panel (V) depicts adsorption perpendicular to the row atop a single Si_2 dimer (fifth icon in Figure 2). Figure 6 illustrates the potential energy versus the distance from the

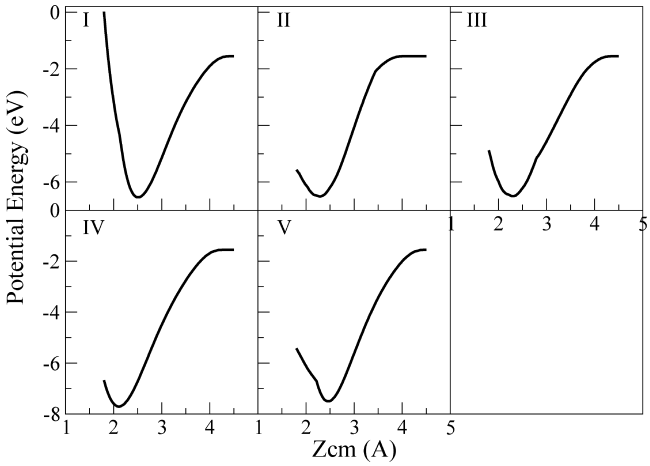

Figure 6. The potential energy versus the distance from the surface at each of the five adsorption sites found in calculations of the reaction dynamics (Figures 2 and 9). The icons of Figure 2 depict schematically the adsorbate orientation in each of the adsorption sites. (I) I_2 attachment parallel to the dimer rows; (II) diagonal attachment, with the I_2 bridging two dimer rows; (III) diagonal attachment along a single dimer row; (IV) adsorption perpendicular to the rows, bridging two rows; (V) adsorption perpendicular to the row, atop a single Si_2 dimer. The potential was minimized with respect to all coordinates other than Z_{cm} at each of the sites and for each value of Z_{cm}.

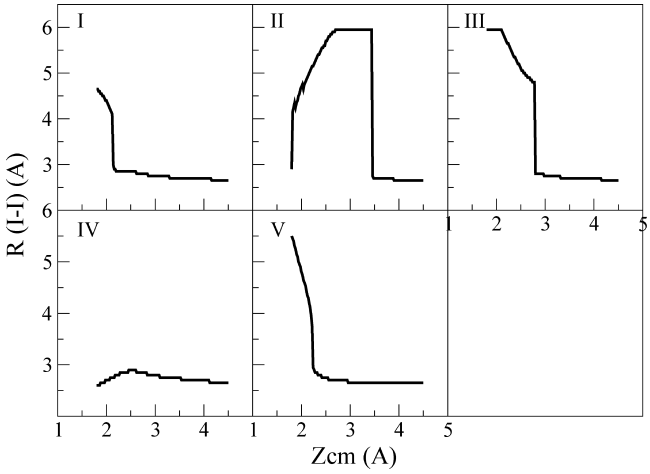

Figure 7. The I−I distance versus the center-of-mass *z*-coordinate at the five adsorption sites considered in Figures 2 and 6.

surface at each of the adsorption sites. The potential was minimized at each configuration with respect to all coordinates other than Z_{cm} at each value of molecule−surface distance Z_{cm}. (Constant terms in the potential were omitted; hence, absolute energies do not have significance, but the relative energy in the different panels does.) As expected from comparison of the gas-phase I_2 equilibrium distance ($r_{eq,I_2} = 2.666$ Å) with the Si−Si distances in Figure 1, the minimum-energy configurations correspond to $\Phi = 0$ for the parallel configuration of panel (I) (left-most icon in Figure 2), $\Phi = \pi/4$ for the diagonal configurations of panels (II) (second icon) and (III) (third icon), and $\Phi = \pi/2$ for the configurations shown in panels (IV) (forth icon) and (V) (fifth icon). Figure 7 complements Figure 6 by illustrating the equilibrium I−I bond distance, $R_{I-I}(Z_{cm})$, versus the center-of-mass *z*-coordinate, Z_{cm}, at each of the configurations. For the configuration of panel (I), $R_{I-I}(Z_{cm})$ remains close to its gas-phase equilibrium value as the molecule approaches the surface and exhibits a sharp increase, corresponding to breakage, at $Z_{cm} = 2.22$ Å. For the diagonal approach of panel (II), where the I_2 axis bridges two dimer rows, the sharp $R_{I-I}(Z_{cm})$

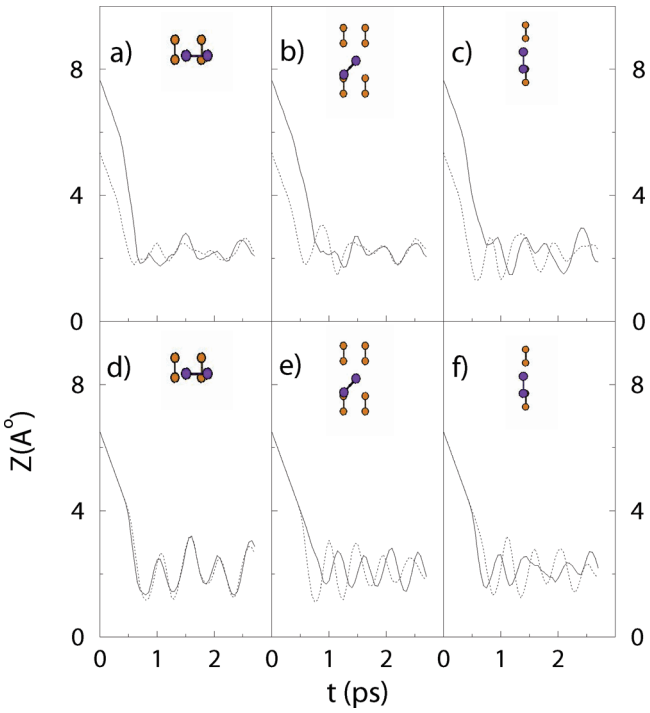

Figure 8. The distance of each of the I atoms from the Si surface versus the time for six trajectories that were initiated with different values of the orientation angles, Θ, Φ, but are identical in other initial conditions. (a and d) $\Phi_i = 0$; (b and e) $\Phi_i = \pi/4$; (c and f) $\Phi_i = \pi/2$. The insets show the final adsorbate orientation resulting from these trajectories and illustrates the way in which the initial gas-phase alignment is imprinted onto the surface patterning.

increase occurs, as expected, at a much larger distance, $Z_{cm} = 3.44$ Å. At this configuration, the I_2 molecule has to elongate substantially beyond its equilibrium configuration already at large distances from the surface in order to interact with both Si atoms (and thus minimize the energy). The interaction with the Si atoms is optimized, and hence, the minimum is reached, only at smaller Z_{cm} values. The diagonal configuration of panel (III) exhibits breakage at $Z_{cm} = 2.78$ Å, whereas the configuration of panel (IV) shows a much more gradual elongation of the I−I bond with decreasing Z_{cm}. Finally, the configuration of panel (V) allows the I−I distance to remain nearly intact well below the equilibrium Z_{cm} value, undergoing a change at $Z_{cm} = 2.12$ Å. Figure 7 agrees with the results of ref 36, where it was experimentally found that orientationally random I_2 molecules adsorb onto Si(100) at the parallel and vertical configurations of panels (I) and (V), respectively, exhibiting breakage in both cases, wherein the atoms retain the configuration of the adsorbed molecule while forming Si−I bonds. (It is important to stress that breakage is used here in a loose sense. As discussed above, the I_2 potential energy curve remains bound up to ∼9.6 Å, and hence, molecular adsorption forming two Si−I bond is, in principle, possible at very low surface temperatures.)

Proceeding to discuss the reaction dynamics subject to the potential energy surface s of Figures 3−6, we show in Figure 8 the time evolution of six trajectories that each contain different physics. The inset in each panel classifies the final outcome of the corresponding trajectory following the scheme of Figures 2, 6, and 7, and the curves give the height of the two I atoms above the surface versus time. The six trajectories differ in the choice of the initial orientation of the gas-phase molecule, (Θ_i, Φ_i). In panels (a) and (d), the azimuthal angle is $\Phi_i = 0$, in panels (b) and (e) $\Phi_i = \pi/4$, and in panels (c) and (f) $\Phi_i = \pi/2$. The lower and upper rows of Figure 8 differ in the initial polar angle Θ_i and hence in the adsorption time scale (vide infra) but not in the final orientation of the adsorbate on the surface. All other initial conditions are kept identical in the six trajectories; the initial velocity is 500 m/sec, directed along the surface normal ($\Theta_{cm} = 0$, $\Phi_{cm} = 0$), and both the rotational temperature of the molecular beam and the surface temperature are zero. The effect of varying these parameters is discussed below. It is observed that with this initial velocity, the reaction outcome is concluded within 1.5−2.5 ps, with a time delay between the formation of the first and second I−Si bonds that depends sensitively on the initial orientation. Small-amplitude vibrations of the I atoms with respect to the surface continue over the period of time considered here. Detailed statistics of the trajectories shows that the time delay for an initial velocity of 500 ms^{-1} is, on average, 130 fs but depends rather sensitively on the initial orientation (Θ_i, Φ_i). The closer the polar angle of approach to the parallel configuration ($\Theta_i = \pi/2$), the shorter the delay between the formation of the first and second bonds and the faster the overall reaction. Trajectories where the initial azimuthal angle is close to $\Phi_i = \pi/4$ (panels (b) and (e)) experience greater repulsion, as expected from comparison of the Si−Si distances in Figure 1 to the I_2 equilibrium distance. These give rise to longer time delays, up to ∼1000 fs, for the smallest Θ_i considered. By contrast, configurations where the approach to the surface is energetically facile, such as $\Phi_i = 0, \pi/2$, correspond to smaller delays, down to ∼50 fs, for $\Theta_i = \pi/2$, and faster overall reaction. While these results are intuitively expected, they illustrate the controllability of the reaction mechanism and dynamics through gas-phase alignment.

The effect of the initial velocity is likewise expected. As v_i increases from 100 to 2000 ms^{-1}, the time delay between formation of the first and second Si−I bonds decreases, and the overall reaction time shortens. With $v_i = 100$ ms^{-1}, the reaction generally does not come to conclusion within the 3 ps trajectories considered here. Clearly, the details of the time evolution of different trajectories with identical initial conditions varies widely, but certain aspects of Figure 8 are characteristic, as will become evident in discussion of the results of a statistical study below.

Our results suggest that the I_2/Si(100) reaction mechanism differs qualitatively from that of the extensively studied F_2/Si(100) analogue. In that latter case, it was found, under comparable conditions to those used here, that one of the main reaction pathways is abstraction, where one F atom attaches to the surface while the other is scattered off.[26] The difference found here is readily understood by inspection of Figure 1. Whereas the F_2 bond length ($r_{eq,F_2} \approx 1.4$ Å) is considerably shorter than the distance between two adjacent atoms in all directions on the Si(100) surface, the I_2 bond length ($r_{eq,I_2} \approx 2.7$ Å) makes a better match with the substrate Si−Si distances.

To determine the probability of adsorption in each of the configurations of Figures 6−8 and explore the extent to which the deposited patterns are controllable through laser alignment, we carried out 6 sets of trajectory calculations for 5 initial velocities and 2 rotational temperatures, considering, for each set, 12 combinations of the polar and azimuthal angles Θ_i, Φ_i. For each set of controlled parameters, a random reaction site was generated using a Monte Carlo technique within the limits of the target area. The initial location of the center of mass above the surface was set to 6.5 Å, and the polar and azimuthal angles of the center-of-mass velocity vector were set to ($\Theta_{cm} = 0$, $\Phi_{cm} = 0$) in all calculations. Our results are clearly independent of the former parameter (provided that it is taken outside of the interaction range) while depending markedly on the latter two.

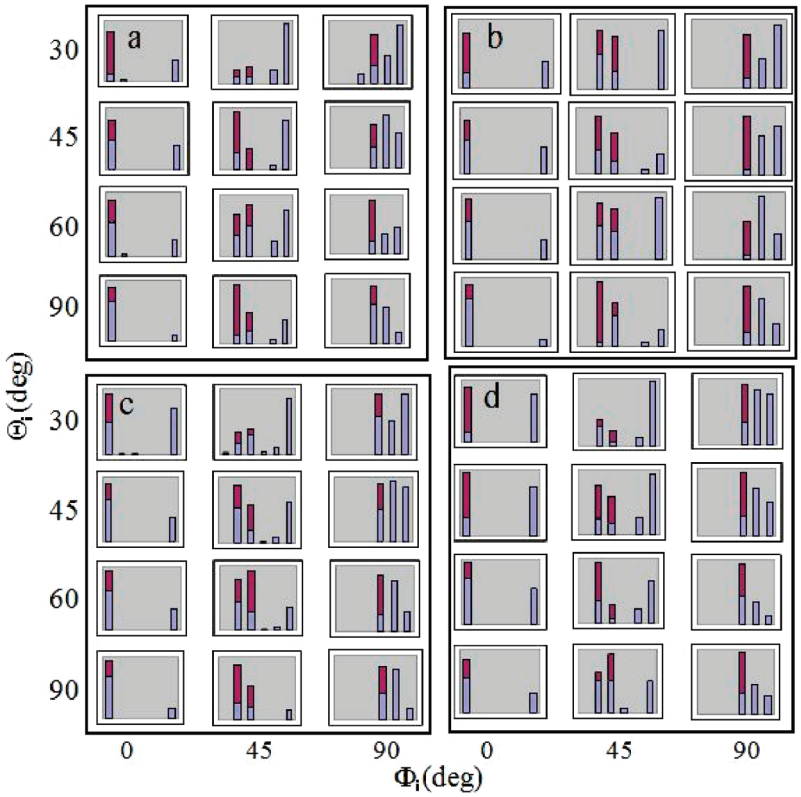

Figure 9. The reaction outcome as a function of the polar and azimuthal angles of the gas-phase projectile. The five first bars from the left provide the adsorption site following the order of Figure 2. The right-most bar indicates the proportion of inconclusive trajectories that did not settle into a definite configuration within the trajectory run time. The upper (dark) part of each bar corresponds to trajectories where only a single Si−I bond formed before the end of the calculation, whereas the lower part corresponds to trajectories where the formation of two Si−I bonds was observed. The initial velocity is (a)100, (b) 800, and (c, d) 1000 ms^{-1}. The rotational temperature is 0 K in (a−c) and 25 K in (d).

Figure 9 summarizes our results in the form of bar graphs of the reaction outcome as a function of the polar and azimuthal angles of the gas-phase projectile. Figure 2 serves as a glossary and associates each one of the five left-most bars with a physical site, as illustrated schematically by the adjacent icon. The left-most five bars in each graph also correspond to the five panels of Figures 6 and 7. The upper (dark) part of each bar gives the proportion of trajectories where only a single Si−I bond formed before the end of the calculation, whereas the lower part corresponds to trajectories where the formation of two Si−I bonds was observed. The sixth (right-most) bar indicates the proportion of inconclusive trajectories that did not settle into a definite configuration within the trajectory run time and serves as a measure of the statistical significance of our results. It is evident that the orientation of the adsorbate on the surface is controllable through gas-phase alignment, despite the strong directional properties of the Si(100) surface. As seen in Figure 9, for $\Phi_i = 0$, the vast majority of trajectories lead to parallel orientation of the adsorbates patterning the surface (adsorption site (I) in Figures 6 and 7 and the left-most icon in Figure 2), whereas for $\Phi_i = \pi/4$, the molecule adsorbs in a diagonal orientation with respect to the dimer rows (adsorption sites (II) and (III) in Figures 6 and 7 and the second icon from the left in Figure 2), and for $\Phi_i = \pi/2$, most trajectories lead to orientation of the adsorbates vertical to the dimer rows. The role played by the initial polar angle Θ_i is similarly evident. As Θ_i increases, the number of inconclusive trajectories falls, and the proportion of trajectories leading to the preferred configuration at each Φ_i increases. These effects are observed at all velocities considered and appear to survive finite rotational temperature (see Figure 9d). We find that the probability of observing a given orientation depends only weakly on the initial velocity, although the details of the trajectory's evolution are velocity-dependent.

Thus, whereas a beam of randomly oriented I_2 molecules adsorbs in a mixture of five configurations, corresponding to three different orientations and with the two energetically preferred configurations strongly dominating, an aligned beam can be directed to adsorb along a desired direction in the surface plane. We remark that, in a related study of the dissociative chemisorption of F_2 on Si(100), the authors found that for molecules incident with their axes parallel to the surface, the relative location of the F atoms on the surface is predominantly determined by the initial alignment of the molecule.[26]

It would be of interest for future numerical work to explore the generality of the effect observed here. It is clear that in cases where the surface and molecular properties combine to single out a unique energetically stable site, the gas-phase alignment will no longer be imprinted onto the adsorption configuration unless the laser-induced potential can be made larger than the field-free potential without causing damage. In such cases, however, the surface properties alone suffice to introduce orientational order, and prealignment of the molecular beam is unnecessary. On the other hand, smooth surfaces, where spontaneous alignment is not expected, will offer greater opportunity for control of the adsorbate alignment via gas-phase alignment than the Si(100) surface.

IV. Conclusions

Our goal in the study described above has been to explore the possibility of applying the molecular alignment induced by a moderately intense, pulsed laser beam to control gas−surface reactions and deposit orientationally ordered nanofeatures on a

surface. To that end, we carried out classical trajectory simulations of the I_2/Si(100) reaction using a fit of ab initio data[46] to the Stillinger−Weber functional form.[21] I_2 is found to adsorb with the molecular axis roughly parallel to the surface plane, independent of the initial alignment of the molecules. The orientation of the molecule in the surface plane is controllable through alignment of the gas-phase projectile. The simplicity of the I_2/Si(100) surface reaction as compared to the well-studied[21−28] F_2/Si(100) analogue originates from the better size match of the I_2 bond length and the Si−Si distances on the Si(100) surface and the less reactive nature of the molecule.

The I_2/Si collision dynamics is a problem of experimental[36,37,42] and potential technological[39] interest in its own right and one that was not studied numerically before. It is important to restress, however, that our goal in the present study has not been to explore the details of the reaction dynamics but rather to use the I_2/Si system as an experimentally relevant but sufficiently simple model system to explore an idea that, we hope, has more general validity. Thus, as stressed in section I, our results are subject to the accuracy of the Stillinger−Weber functional form and to the validity of classical mechanics. We feel, however, that this study suffices to suggest the feasibility of transferring the alignment of gas-phase molecules to the orientational order of adsorbates.

This study should be taken in context with the long-standing interest of chemical dynamics in the stereochemistry of surface collisions, the much more recent but increasingly rapid advance of the experimental technology of aligning and focusing molecules with intense lasers, and the growing interest in new materials with controlled properties. While the prospect of technological applications of the surface reaction of aligned molecules remains to be explored, its potential as a tool for understanding and controlling surface dynamics is inviting.

Acknowledgment. The authors are indented to Prof. Qiang Cui for providing them with the ab initio I_2/Si data prior to publication and for helpful conversations. The research summarized in this publication was carried out in the course of several summers by a group of summer undergraduate students, supported by the National Research Council (NRC) of Canada (A.L., D.S., and S.B.), the Materials Research Science and Engineering Center (MRSEC) at Northwestern University under a Research Experience for Undergraduates (REU) program (N. W.), and the Summer Research Opportunities Program (SROP) for minority undergraduate students at Northwestern University (D.S.). The authors are grateful to these programs for enabling this research.

Supporting Information Available: In the Supporting Information, we report several results that, while not necessary for conveying our main message, may interest the in-depth reader. This material is available free of charge via the Internet at http://pubs.acs.org.

References and Notes

(1) Cho, V. A.; Bernstein, R. B. *J. Chem. Phys.* **1991**, *95*, 8129.
(2) Seideman, T. *J. Chem. Phys.* **1995**, *103*, 7887–7896.
(3) Ortigoso, J.; Rodrígues, M.; Gupta, M.; Friedrich, B. *J. Chem. Phys.* **1999**, *110*, 3870–3875.
(4) Haj-Yedder, A. B.; Auger, A.; Dion, C. M.; Cance's, E.; Keller, A.; Bris, C. L.; Atabek, O. *Phys. Rev. A* **2002**, *66*, 063401.
(5) Daems, D.; Guerin, S.; Hertz, E.; Jauslin, H. R.; Lavorel, B.; Faucher, O. *Phys. Rev. Lett.* **2005**, *95*, 063005.
(6) Rosca-Pruna, F.; Vrakking, M. J. J. *Phys. Rev. Lett.* **2001**, *87*, 153902.
(7) Leibscher, M.; Averbukh, I. S.; Rabitz, H. *Phys. Rev. Lett.* **2003**, *90*, 213001.
(8) Stapelfeldt, H.; Seideman, T. *Rev. Mod. Phys.* **2003**, *75*, 543–557.
(9) Seideman, T.; Hamilton, E. *Adv. At., Mol., Opt. Phys.* **2006**, *52*, 289–329.
(10) Seideman, T. *Phys. Rev. A* **1997**, *56*, R17.
(11) Gordon, R.; Zhu, L.; Schroeder, A.; Seideman, T. *J. Appl. Phys.* **2003**, *94*, 669.
(12) Yan, Z.-C.; Seideman, T. *J. Chem. Phys.* **1999**, *111*, 4113–4120.
(13) Underwood, J. G.; Spanner, M.; Ivanov, M. Y.; Mottershead, J.; Sussman, B. J.; Stolow, A. *Phys. Rev. Lett.* **2003**, *90*, 223001.
(14) Seideman, T. *Phys. Rev. Lett.* **1999**, *83*, 4971–4974.
(15) Parker, D. H.; Bernstein, R. B. *Annu. Rev. Phys. Chem.* **1989**, *40*, 561.
(16) Seideman, T. *J. Chem. Phys.* **1997**, *107*, 10420–10429.
(17) Stapelfeldt, H.; Sakai, H.; Constant, E.; Corkum, P. B. *Phys. Rev. Lett.* **1997**, *79*, 2787.
(18) Engstrom, J. R.; Nelson, M. M.; Engel, T. *Surf. Sci.* **1989**, *215*, 437.
(19) Li, Y. L.; Pullman, D. P.; Yang, J. J.; Tsekouras, A. A.; Gosalve, D. G.; Laughlin, K. B.; Zhang, Z.; Schulberg, M. T.; Gladstone, D. J.; Mcgonigal, M.; Ceyer, S. T. *Phys. Rev. Lett.* **1995**, *74*, 2603.
(20) Behringer, E. R.; Flaum, H. C.; Kummel, A. C. *J. Phys. Chem.* **1995**, *99*, 5533.
(21) Weber, T. A.; Stillinger, F. *J. Chem. Phys.* **1990**, *92*, 6239.
(22) Weakliem, P.; Wu, C.; Carter, E. *Phys. Rev. Lett.* **1992**, *69*, 200.
(23) Weakliem, P.; Wu, C.; Carter, E. *Phys. Rev. Lett.* **1992**, *69*, 1475.
(24) Wu, C.; Carter, E. *Phys. Rev. B* **1992**, *45*, 9065.
(25) Weakliem, P.; Carter, E. *J. Chem. Phys.* **1993**, *98*, 737.
(26) Carter, L.; Khodabandeh, S.; Weakliem, P. C.; Carter, E. *J. Chem. Phys.* **1994**, *100*, 2277.
(27) Carter, L.; Carter, E. *J. Phys. Chem.* **1996**, *100*, 873.
(28) Carter, L.; Carter, E. *Surf. Sci.* **1996**, *360*, 200.
(29) Szabo, A.; Engel, T. *J. Vac. Sci. Technol., A* **1994**, *12*, 648.
(30) Teraoka, Y.; Nishiyama, I. *Appl. Phys. Lett.* **1993**, *63*, 3355.
(31) Sullivan, D. J. D.; Flaum, H. C.; Kummel, A. C. *J. Phys. Chem.* **1993**, *97*, 12051.
(32) Vita, A. D.; Stich, I.; Gillan, M. J.; Payne, M. C.; Clarke, L. J. *Phys. Rev. Lett.* **1993**, *71*, 1276.
(33) Feil, H.; Dieleman, J.; Garrison, B. J. *J. Appl. Phys.* **1993**, *74*, 1303.
(34) Stich, I.; Vita, A. D.; Payne, M. C.; Gillan, M. J.; Clarke, L. J. *Phys. Rev. B* **1994**, *49*, 8076.
(35) Xu, G. J.; Graugnard, E.; Trenhaile, B. R.; Nakayama, K. S.; Weaver, J. H. *Phys. Rev. B* **2003**, *68*, 075301.
(36) Rioux, D.; Stepniak, F.; Pechman, R. J.; Weaver, J. H. *Phys. Rev. B* **1995**, *51*, 10981.
(37) Xu, G. J.; Zarkevich, N. A.; Agrawal, A.; Signor, A.; Trenhaile, B. R.; Johnson, D. D.; Weaver, J. H. *Phys. Rev. B* **2005**, *71*, 115332.
(38) Zarkevich, N.; Johnson, D. *Surf. Sci.* **2005**, *591*, L292.
(39) Cai, W.; Lin, Z.; Strother, T.; Smith, L. M.; Hamers, R. J. *J. Phys. Chem. B* **2002**, *106*, 2656.
(40) Msaad, H.; Michel, J.; Lappe, J. J.; Kimerling, L. C. *J. Electron. Mater.* **1994**, *23*, 487.
(41) Bulanin, K. M.; Shah, A. G.; Fitzgeral, D. R.; Doren, D. J.; Teplyakov, A. V. *J. Phys. Chem. B* **2002**, *106*, 7286.
(42) Aldao, C.; Weaver, J. *Prog. Surf. Sci.* **2001**, *68*, 189.
(43) McNab, I. R.; Polanyi, J. C. *Chem. Rev.* **2006**, *106*, 4321.
(44) Guo, H.; Ji, W.; Polanyi, J. C.; Yang, J. S. Y. *ACS Nano* **2008**, *2*, 699.
(45) Frenkel, D.; Smit, B. *Understanding Molecular Simulation*; Academic Press: New York, 2002.
(46) Cui, Q. Ph. D. Thesis; Emory University: Atlanta, GA, 1997.
(47) Richards, W. G.; Barrow, R. F. *Trans. Faraday Soc.* **1964**, *60*, 797.

JP9120113